Photonics **2015**, *2*, 164-183; doi:10.3390/photonics2010164

OPEN ACCESS

photonics

ISSN 2304-6732

www.mdpi.com/journal/photonics

Article

Optimum Pump Pulse Duration for X-Ray Ar-Plasma Lasing

Leili Masoudnia [1,*] and Davide Bleiner [1,2]

[1] Empa- Swiss Federal Laboratories for Materials Science and Technology, Überlandstrasse 129, Dübendorf CH-8600, Switzerland; E-Mail: davide.bleiner@empa.ch

[2] Institute of Applied Physics, University of Bern, Sidlerstrasse 5, Bern CH-3012, Switzerland

* Author to whom correspondence should be addressed; E-Mail: leili.masoudnia@empa.ch; Tel.: +41-58-765-6126.

Received: 22 December 2014 / Accepted: 29 January 2015 / Published: 10 February 2015

Abstract: In plasma-driven X-ray lasers, it is critical to optimize the duration and time delay between pump pulses. In this study, we have done parametric simulations in order to systematically investigate the optimum time configuration of pump pulses. Here, we are mainly interested in soft X-ray lasers created using a Ar target irradiated with laser pulses, which operate at a wavelength $\lambda = 46.9$ nm in the $2p^5 3p^1 (J = 0) \rightarrow 2p^5 3s^1 (J = 1)$ laser transition. It is shown that the optimum time scale required to achieve Ne-like ions, as well as the time required to generate a population inversion depend on the combined effect of the electron temperature and electron density. The electron density and temperature are respectively a factor of $\approx$2.1- and $\approx$5-times higher in the case of a short pulse of 0.1 ps in comparison to a long pulse of 1,000 ps (at a constant fluence). The most effective lasing happens with short pulses with a pulse duration comparable to the total relaxation time from the upper level, namely $\Delta\tau_p \leq 35$ ps. Power laws to predict the optimum laser intensity to achieve Ne-like Ar^{+8} are obtained.

Keywords: plasma-driven X-ray lasers; Ar^0 target; ionization time; pumping time; relaxation time

PACS classifications: 52.38.-r; 52.65.-y; 52.38.Ph; 52.25.-b

---

1. Introduction

A number of ways have been proposed to increase the efficiency of laser-irradiated solid targets for plasma-driven X-ray lasing [1]. The main drawback of solid targets, however, is the presence of strong density gradients, which cause the refraction of the pump pulse, limiting the gain [2,3]. A solution to the strong density gradients we have studied is using hohlraum targets [2].

Alternatively, gas targets have several advantages over solid targets, such as the soft density gradients, lack of debris, high repetition rate and long unbroken operation [4–10]. For the first time, the generation of laser radiation with Ar^0 gas at a wavelength of 46.9 nm producing a gain of 0.6 cm^{-1} was observed in a capillary discharge by Rocca *et al.* [11].

In the laser-produced gas targets, the possibility of having a high repetition rate will lead to high average power for soft X-ray lasers. Besides, the advantage of the compact size and the low cost in comparison to the large-scale X-ray sources, such as free electron lasers [12] and synchrotron facilities [13], is important.

Table 1 summarizes the operating conditions used experimentally in the lasing of the Ne-like Ar^{+8} plasma at $\lambda = 46.9$ nm in the $2p^5 3p^1 (J = 0) \rightarrow 2p^5 3s^1 (J = 1)$ laser transition [5–10]. In references [5–10], the plasma is produced with a long pulse ($\Delta\tau_{MP} = 450$ ps), a combination of a long ($\Delta\tau_{PP} = 600$ ps) and a short pulse ($\Delta\tau_{MP} = 6$ ps) and double-short pulses ($\Delta\tau_{PP} = \Delta\tau_{MP} = 1.5$ ps). Here, the "short pulse" means a pulse with a pulse-duration shorter or in the order of the lifetime of the upper level (lasing level). On the other hand, the "long pulse" has a pulse duration longer than the lifetime of the upper level. The lifetime of the upper level, taking into account the radiative decay (without considering collisional processes) in Ne-like Ar^{+8}, is ≈100 ps (see Figure 1). Table 1 shows the gain due to the collisional excitation calculated by fitting the Linford formula [14] to the experimental data. It shows that the highest gain coefficient is 18.7 cm^{-1}, achieved in the case of plasma driven with double-short pulses [10]. As the population inversion only persists as long as the plasma parameters are close to optimum [15], then for long pumping, the plasma will destroy the gain, and most of the possible inversions would be lost by spontaneous emission.

Table 1. A summary of the experimental-operating conditions in the lasing of the Ne-like Ar^{+8} plasma at $\lambda = 46.9$ nm. Legend: $\Delta\tau_{PP}$, $\Delta\tau_{MP}$ and Δt stand for the pulse duration of the pre-pulse, the pulse duration of the main pulse and the time delay between two pulses (pulse to pulse separation), respectively. λ_P, I_{PP} and I_{MP} stand for the pump laser's wavelength, the pre-pulse-laser intensity and the main-pulse-laser intensity at the focusing point on the target, respectively. ρ_0 and g stand for the initial gas density of Ar^0 and the gain coefficient, respectively.

$\Delta\tau_{PP}$ (ps)	$\Delta\tau_{MP}$ (ps)	Δt (ps)	λ_P (nm)	I_{PP} (W/cm^2)	I_{MP} (W/cm^2)	ρ_0 (mg/cm^3)	g (cm^{-1})	Ref
-	450	-	1,315	-	$5 \cdot 10^{12}$–$3 \cdot 10^{13}$	0.15	1.65	[5,6]
600	6	500–2,100	1,054	$2 \cdot 10^{11}$	$5 \cdot 10^{13}$	4	11	[7–9]
1.5	1.5	1,200	1,054	$7 \cdot 10^{14}$	$4.7 \cdot 10^{15}$	0.166	18.7	[10]

Table 1 shows that the time delays between pulses are in the range of 500–2,100 ps, which is to achieve the optimum ionization level. The wavelength of pump lasers are either 1,054 nm or 1,315 nm,

and the initial Ar^0 mass densities are in the range of 0.15–4 mg/cm^3. In [5,6], a pulse with intensity in the range of $5 \cdot 10^{12}$–$3 \cdot 10^{13}$ W/cm^2 is used to ionize the plasma up to the required ionization stage to produce a lasing plasma. In [7–9], a pulse with lower intensity $2 \cdot 10^{11}$ W/cm^2 produces a pre-plasma, and then, a pulse with higher intensity $5 \cdot 10^{13}$ W/cm^2 produces the lasing plasma. In [10], double pico-second pulses with intensity $7 \cdot 10^{14}$ W/cm^2 and $4.7 \cdot 10^{15}$ W/cm^2 rapidly produce the pre-plasma and heat it. In the plasma-driven X-ray laser, it is critical to optimize the duration and time delay (timing) between pump pulses.

All of the so far reported optimization in Ar comes from experimental studies [5–10], which had a lack of theoretical analysis. The aim of this work is to present parametric simulations in order to systematically investigate the optimum timing configuration of pump pulses.

This work is organized as follows: In Section 2, a description of modeling codes and boundary conditions is given. In Section 3, the approach used in the theoretical calculation is explained. In Section 4.1.1, the collisional ionization time of a neutral Ar^0 is calculated. In Section 4.1.2, the time required to produce Ne-like ions is discussed. In Section 4.1.3, the transition times among excited levels are calculated. In Section 4.1.4, the required time to achieve a population inversion and the relaxation time from excited levels are obtained. In Section 4.2, we show how the pulse duration can affect the evolution of the electron density and temperature, which affect the time required for the production of the Ne-like Ar^{+8}, the time scale of the pumping and the relaxation time. In Section 4.3, the optimum pump laser intensity with dependency on the pulse duration and initial gas density in order to have Ne-like Ar^{+8} is obtained.

2. Modeling Codes

2.1. Atomic Physics Code

The flexible atomic code (FAC) [16] was used to calculate the required atomic data, such as collisional excitation coefficients and spontaneous emission coefficients. FAC employs a fully relativistic approach based on the Dirac equation. It is a configuration interaction program for calculating atomic collisional and radiative processes, including (i) energy levels, (ii) radiative transitions and the inverse process of (iii) photo-excitation, (iv) collisional excitation and (v) ionization by electron impact and its inverse process (vi) collisional de-excitation and (vii) three-body recombination, (viii) radiative recombination and its inverse process (ix) photo-ionization, (x) auto-ionization and its inverse process and (xi) dielectronic capture. These are indeed the required coefficients we need to solve the non local thermodynamic equilibrium (NLTE) system of rate equations. Furthermore, FAC has been extensively used before for calculating atomic data by several publications [17–20].

Due to some limitations of FAC in handling the calculation of ionic distributions, the FLYCHK code from the NIST was used, too. The FLYCHK code was used to calculate ionic level populations by a solving multi-level rate equation in zero dimension, as explained extensively elsewhere [21,22].

2.2. Hydro-Code

"Hyades" [23] is a one-dimensional, three-geometry (planar, cylindrical or spherical), three-fluid (electrons, ions and radiation) hydrodynamics simulation code. The conservation equations for mass, momentum and energy are solved in a Lagrangian coordinate system. The three fluids are treated individually in a fluid approximation, each having its own temperature. Each fluid is assumed to be in LTE, which is to say that the electrons and the ions are described well in the classical limit by Maxwell–Boltzmann statistics, and the radiation field is Planckian. Electron degeneracy effects, important in low-temperature, high-density plasmas, are taken into account. The equation of state (EOS) and related thermodynamic coefficients are obtained from external tables that have been compiled using experimental data and theoretical models. The energy transport by free-electrons and ions is modeled in the flux-limited diffusion approximation (the default value for both electrons and ions is 0.4). Radiation is transported according to the photon energy, *i.e.*, ultra-violet and soft X-rays have very short mean free paths, while the more energetic photons' harder X-rays will penetrate deeply into the material. The absorption and emission coefficients are determined self-consistently from the atomic physics model of choice or may be supplied by the user in tabular form. The absorption of laser light by a hot plasma is dominated by inverse Bremsstrahlung at the intensity of interest to this work.

2.3. Boundary Conditions

In Sections 4.2 and 4.3, a gas target, such as Ar^0, considering an electronic flux-limit multiplier of 0.05 and a multi-group radiation transport of 50 groups (in Hyades), is studied. The plasma is created using $\lambda = 1054$-nm Nd:glass laser (IR pulse) with a Gaussian pulse shape. The pump pulse is irradiated at an angle of 90° (normal incidence) to the target. The arrival time of the peak of Gaussian pulse on the target is considered two-times the pulse duration. Here, the considered geometry is planar (1D Cartesian) geometry. In Section 4.2, the initial gas density of neutral Ar^0 at all zones (irradiated area) is considered the same, which is 4 mg/cm^3 ($6 \cdot 10^{19}$ cm^{-3}).

3. Theoretical Background

The main computational steps of the approach used in our study are (i) calculation of the ionization time and (ii) transition time and (iii) calculation of the pumping and relaxation time. These are needed to quantify the optimum timing for the pump pulses.

3.1. Ionization Time

The ionization time as given by McWhirter's condition [24] is: $t[s] = 10^{12}/n_e$ (cm^{-3}). For this calculation, McWhirter [24] considered two processes: (i) collisional ionization; and (ii) radiative recombination. However, Pert [25] pointed out that McWhirter's criterion is overestimated by up to a factor of 10. Here, our analysis for estimating the ionization time includes the following processes: (i) collisional ionization; (ii) three-body; (iii) radiative; and (iv) dielectronic recombination. The quantity of the ionization time can be obtained considering a two-level system, in which transitions take place

from one level to the other, and the solution characterized by an initial transient phase, during which the one charge level (Ar^{+Z}) will be ionized to the higher charge level ($Ar^{+(Z+1)}$) [24]. Solving rate equations [24] at the steady state, where $Ar^{+(Z+1)} \propto Ar^{+Z}(1 - e^{-tn_e(S_Z+\alpha_{Z+1}+n_e\beta_{Z+1}+D_{Z+1})})$, gives the ionization time between two adjacent states as follows:

$$t_{Ar^{+Z}\rightarrow Ar^{+(Z+1)}}[s] = \frac{1}{n_e(S_Z + \alpha_{Z+1} + n_e\beta_{Z+1} + D_{Z+1})} \quad (1)$$

where n_e is expressed in cm^{-3} and the collisional ionization rate S_Z from charge state Z to $Z + 1$ [24] in cm^3s^{-1}. The terms α_{Z+1}, β_{Z+1} and D_{Z+1} are, respectively, the radiative, collisional three-body and dielectronic recombination rates [28,29] applied to the ionic charge level Z + 1 in cm^3s^{-1}, cm^3s^{-1}/cm^{-3} and cm^3s^{-1}, respectively. It is mentionable that Equation (1) gives the ionization time (characteristic time) when $Ar^{+(Z+1)}$ has ≈63% of the Ar^{+Z} population.

3.2. Cooling Time

The characteristic timescale for radiative cooling is of the same order as the time it takes for the plasma to reach thermal equilibrium [26]. The equilibrium time t_{eq} of the plasma is predicted as follows [27]:

$$t_{eq}[s] \approx 3.16 \cdot 10^{-10} \frac{A}{Z^2}\left(\frac{kT_e}{100}\right)^{3/2}\left(\frac{10^{21}}{n_i log[(\frac{3}{2\bar{z}^2}) \cdot (\frac{(kT_e)^3}{\pi e^6 n_e})^{1/2}]}\right) \quad (2)$$

where A is the atomic weight of the ions, Z is the atomic number, $\bar{z}$ is the average charge state, kT_e is the electron temperature in eV, n_e is the electron density in cm^{-3} and n_i is the ion density.

3.3. Transition Times

Due to the selection rules, the transition from ground level (J = 0) to the upper level (J = 0) is only achieved by the monopole collisional excitation (Figure 1).

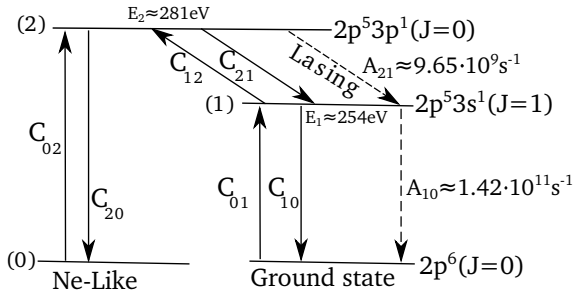

Figure 1. Grotrian scheme and the transitions for the lasing of the Ne-like Ar^{+8}. The energy levels schematically are composed of the upper (2) and lower (1) lasing levels and the ground (0) level.

The X-ray produced across a plasma follows transition times as follows:

$$\begin{aligned}
\tau_{02}[s] &= \frac{1}{n_e C_{02}} \\
\tau_{01}[s] &= \frac{1}{n_e C_{01}} \\
\tau_{12}[s] &= \frac{1}{n_e C_{12}} \\
\tau_{20}[s] &= \frac{1}{n_e C_{20}} \\
\tau_{10}[s] &= \frac{1}{A_{10} + n_e C_{10}} \\
\tau_{21}[s] &= \frac{1}{A_{21} + n_e C_{21}}
\end{aligned} \tag{3}$$

where n_e is in cm^{-3}, A_{ij} in s^{-1} and C_{ij} in cm^{3}s^{-1}. Here, τ_{02} is the transition time from the ground level (0) to the upper level (2), τ_{01} is the transition time from the ground level (0) to the lower level (1), *etc*. In the transition time from the upper level (2) to the lower level (1) and from the lower level (1) to the ground level (0), the radiative decays (A_{21} and A_{10}) are also allowed. In fact, the τ_{10} and τ_{21} depend on both radiative decay and collisional de-excitation if both are of the same order of magnitude. Otherwise, the τ_{10} and τ_{21} depend only on the largest one, which means a shorter time.

The electron collisional excitation rates (C^e_{ij}) between levels depend on the electron temperature [30]:

$$C^e_{ij}[cm^3 s^{-1}] = 1.6 \cdot 10^{-5} \frac{< g_{ij} >}{(kT_e)^{1/2}} \frac{f_{ij}}{\Delta E_{ij}} e^{(-\Delta E_{ij}/kT_e)} \tag{4}$$

where f_{ij} is the oscillator strength, ΔE_{ij} is the excitation energy and $< g_{ij} >$ is the Gaunt factor. For calculating the collisional de-excitation rate (C^d_{ji}), considering detailed balancing [31,32], one has that:

$$C^d_{ji}[cm^3 s^{-1}] = \frac{\gamma_i}{\gamma_j} C_{ij}{}^e e^{(\Delta E_{ij}/kT_e)} \tag{5}$$

3.4. Pumping and Relaxation Time

The populations of the Ne-like levels are computed in a three-level model [33,34]; Figure 1. Oliva *et al.* have shown [33] that a three-level model has good agreement with their experimental data. In their model, they took into account only Doppler broadening, while collisional broadening should also be treated. Here, in our calculation, we take into account both Doppler broadening and collisional broadening. If n_2 and n_1 are the upper and lower laser level populations (Figure 1) and σ_{stim} is the cross-section for the stimulated emission, the small signal gain at $\lambda = \lambda_0$ (λ_0 is 46.9 nm for a Ne-like Ar^{+8} laser) is found as follows [35]:

$$g_0(\lambda = \lambda_0) = n_2 F \sigma_{stim}(\lambda = \lambda_0) \tag{6}$$

where F is the population inversion factor, defined as follows:

$$F = 1 - (\frac{\gamma_2}{\gamma_1}) \frac{n_1}{n_2} \tag{7}$$

where γ_i, γ_j are the degeneracies of the i-th, j-th levels, and the degeneracy of each level is 2J + 1. Here, we compute the value of the gain at the center of line profile $\lambda = \lambda_0$.

The cross-section σ_{stim} is given by [30]:

$$\sigma_{stim} = \frac{\pi r_0 f_{lu} \lambda}{\Delta\lambda_x} \frac{\gamma_l}{\gamma_u} \varphi_x(\lambda) \tag{8}$$

where $\Delta\lambda_x$ is the spectral line width and $\varphi_x(\lambda)$ is the normalized line shape profile. Line shape $\varphi_x(\lambda)$ is given by the convolution integral,

$$\varphi_x(\lambda) = \int_{-\infty}^{+\infty} \varphi_G(\lambda)\varphi_L(\lambda_0 - \lambda)d\lambda \tag{9}$$

Assume that Doppler broadening (φ_G) and collisional broadening (φ_L) act on a line profile simultaneously; then, the resulting measured line shape is a Voigt profile. In a plasma, Doppler broadening due to the thermal motion of ions produces a Gaussian-shaped line function, where $\Delta\lambda_D = \frac{\sqrt{2kT_i/M}}{c}\lambda$ is the Doppler width; where kT_i is the ion temperature and M is the ion mass. The value of the spectral bandwidth for the full width at half maximum of this Gaussian intensity is given by [36]:

$$\Delta\lambda_G = 2\sqrt{2ln2}\Delta\lambda_D \tag{10}$$

The formula for the electron impact broadening is used to estimate [37]:

$$\Delta\lambda_L = 2 \cdot 10^{-16} w n_e [1 + 1.75 \cdot 10^{-4} \alpha n_e^{1/4} (1 - 0.00062 n_e^{1/6} T_e^{-1/2})] \tag{11}$$

Here, T_e in eV and n_e are in cm^{-3}; where α is the ion broadening parameter and w is an electron impact width.

The FWHM of the Voigt profile (the convolution of the Lorentzian and Gaussian profile) can be estimated with an accuracy of 0.02% as [38]:

$$\Delta\lambda_x = \Delta\lambda_V \approx 0.5346\Delta\lambda_L + \sqrt{0.2166\Delta\lambda_L^2 + \Delta\lambda_G^2} \tag{12}$$

The populations of the lower (n_1) and upper (n_2) laser level populations can be obtained by solving the stationary rate equations of a three-level model [2,15]:

$$\begin{aligned} \frac{dn_1}{dt} &= -R_1 + P_1 \\ \frac{dn_2}{dt} &= -R_2 + P_2 \end{aligned} \tag{13}$$

where:

$$\begin{aligned} R_1 &= n_1\big(n_e(C_{12} + C_{10}) + A_{10}\big) \\ P_1 &= n_e\left(n_0 C_{01} + n_2 C_{21}\right) + n_2 A_{21} \\ R_2 &= n_2\big(n_e(C_{21} + C_{20}) + A_{21}\big) \\ P_2 &= n_e\left(n_0 C_{02} + n_1 C_{12}\right) \end{aligned}$$

Here, R_1 and R_2 stand for the relaxation rate from the lower level and upper level, respectively. P_1 and P_2 stand for the pumping rate to the lower level and upper level, respectively. The pumping rate to the lower level P_1 includes both collisional excitation from the ground level and collisional de-excitation and radiative decay from the upper level to the lower level. Meanwhile, the pumping rate to the upper level P_2 includes collisional excitation from the ground level and the lower level to the upper level. Here, n_0 is the population in the ground level, *i.e.*, $2p^6$ in the Ne-like system. The quasi-neutral approximation implies that $n_0 = n_e/Z$, where Z is the ion charge. In other words, the population of Ne-like Ar^{+8} at $n_e = 10^{18}$ cm^{-3} is considered $n_0 = 1.25 \cdot 10^{17}$ cm^{-3}.

At a specific electron temperature and density, the pumping time from the Ne-like ground level and the relaxation time to the Ne-like level can be calculated as follows:

$$t_{pum\boldsymbol{i}} = \frac{n_{\boldsymbol{i}}}{\frac{dn_i}{dt}|_{pum\boldsymbol{i}}} \tag{14a}$$

$$t_{rel\boldsymbol{i}} = \frac{n_{\boldsymbol{i}}}{\frac{dn_i}{dt}|_{rel\boldsymbol{i}}} \tag{14b}$$

where $\boldsymbol{i}$ can be considered either as one or two, corresponding to the lower level and upper level, respectively (Figure 1). Additionally, the $\frac{dn_i}{dt}|_{pum\boldsymbol{i}}$ and $\frac{dn_i}{dt}|_{rel\boldsymbol{i}}$ can be considered as follows: $\frac{dn_i}{dt}|_{pum\boldsymbol{i}} = P_i$ and $\frac{dn_i}{dt}|_{rel\boldsymbol{i}} = R_i$, where R_i and P_i are tabulated in Equation (13).

Taking into account Equation (14), the pumping time to the upper (t_{pum2}) and lower level (t_{pum1}) and the relaxation time from the upper level (t_{rel2}) and lower level (t_{rel1}) can be calculated.

Equation (14a) shows that the pumping time to the upper level (t_{pum2}) and lower level (t_{pum1}) depends on the population of the upper and lower levels (n_2 and n_1). Besides, Equation (14b) shows that the relaxation time from the upper level (t_{rel2}) and lower level (t_{rel1}) does not depend on the population of the upper and lower levels (n_2 and n_1).

4. Results and Discussion

For X-ray Ar-plasma lasing, parametric simulations are done, in order to systematically investigate the optimum time configuration of pump pulses. The approach is: (i) calculate the time scales for lasing, including the ionization time, pumping time and relaxation time; (ii) obtain the effect of pulse duration on the electron density and temperature of the laser-produced plasma, which have a combined effect on the time scales for plasma lasing; and (iii) study the effect of pulse shape on the X-ray lasing in Ne-like Ar^{+8}.

4.1. Time Scales for the Plasma Lasing

The characterizing times are: (i) the ionization time of a neutral Ar^0; (ii) the ionization time up to Ne-like Ar^{+8}; (iii) the transition time among excited levels; and (iv) the pumping time and relaxation time among excited levels of Ne-like Ar^{+8}.

4.1.1. Ionization Time of Neutral Ar^0

In this section, we calculate the electron impact ionization time of neutral Ar^0 using the collisional ionization rate recommended by Voronov [39].

Figure 2 shows that the collisional ionization time of a neutral Ar^0 is dependent on the initial electron temperature and density of the pre-plasma. It shows that the ionization time of a neutral Ar^0 by electron impact scales down linearly with electron density. Besides, it shows that for $T_e \geqslant 10$ eV, the electron impact ionization time of the neutral Ar^0 will decrease by a factor as high as 6.8 with increasing electron temperature by a factor of 10. For $T_e < 10$ eV, the electron impact ionization time of the neutral Ar^0 will decrease as high as 3.5 orders of magnitude with increasing electron temperature by a factor of two. Namely, at $T_e < 10$ eV, the collisional ionization time decreases faster by increasing the electron temperature.

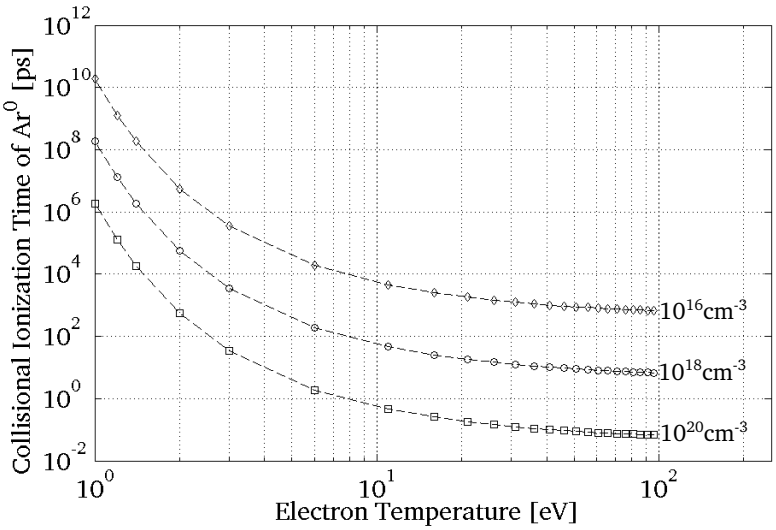

Figure 2. Collisional ionization time of the neutral Ar^0 as a function of the initial electron temperature for a selection of electron densities.

In the next step, we estimate the time required to produce Ne-like Ar^{+8}.

4.1.2. Ionization Time Up to Ne-Like Stage Ar^{+8}

In this section, the ionization time for achieving Ar^{+8} is calculated by using Equation (1), which includes the following important processes: (i) collisional ionization; (ii) three-body; and (iii) radiative, and (iv) dielectronic recombination.

Figure 3 shows the time required for the ionization from Ar^{+6} to Ar^{+7}, Ar^{+7} to Ar^{+8} and Ar^{+8} to Ar^{+9} for different electron temperatures without (a) and with (b) considering the dielectronic recombination effect at optimum electron density [30]. Elton [30] has reported an optimum electron density and temperature for the lasing of Ne-like Ar^{+8}, which are $n_e = 1.5 \cdot 10^{19}$ cm^{-3} and $T_e = 154$ eV, respectively. Dielectronic recombination has a stronger effect on the ionization time of Ar^{+Z} to have Ar^{+8} at electron temperatures less than 50 eV. At these temperature, the ionization time to achieve Ar^{+8} without (a) considering dielectronic recombination is higher than with (b) considering the effect of dielectronic recombination as high as a factor of 30. At electron temperatures $T_e > 50$, the effect of dielectronic recombination to have Ar^{+8} is negligible, and the difference is as low as 14%. However, it has an effect in order to achieve Ar^{+9}.

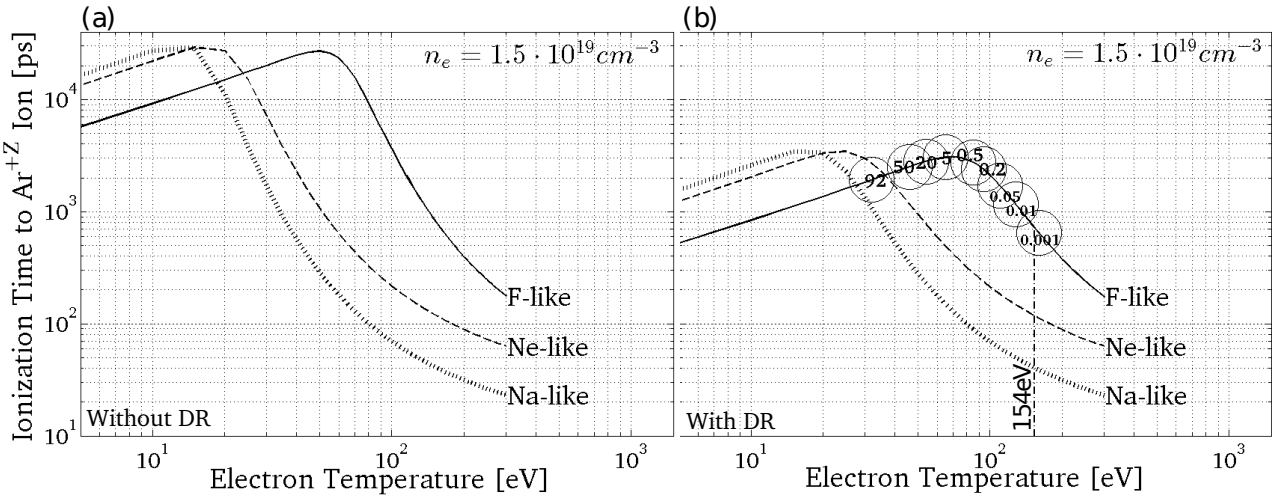

Figure 3. Time required to achieve the Ar^{+Z} ion for the following steps: (i) $Ar^{+6} \rightarrow Ar^{+7}$ (Na-like); (ii) $Ar^{+7} \rightarrow Ar^{+8}$ (Ne-like); and (iii) $Ar^{+8} \rightarrow Ar^{+9}$ (F-like); as a function of temperature at a constant electron density $n_e = 1.5 \cdot 10^{19}$ cm^{-3}. The ionization time without (**a**) and with (**b**) taking the dielectronic recombination (DR) into consideration is shown. The ionic fractions of Ar^{+8} at each specific electron temperature are given on the curve $Ar^{+8} \rightarrow Ar^{+9}$ (F-like).

The vertical line cross of the optimum electron temperature is shown in Figure 3b. It shows that the times required for the ionization from Ar^{+6} to Ar^{+7}, Ar^{+7} to Ar^{+8} and Ar^{+8} to Ar^{+9} are, respectively, 41 ps, 121 ps, and 691 ps.

Inside the circles of Figure 3b, the ionic abundance of Ar^{+8} when the equilibrium state is reached at specific electron temperatures is given (curve: Ar^{+8} to Ar^{+9}). It shows that by increasing the electron temperature, the ionic abundance decreases. Besides, it shows that the plasma requires time to produce Ne-like ions. With increasing electron temperatures, the time required for ionization time between levels to be achieved is getting shorter, and the abundance of Ne-like ions is getting smaller, which can result in a low conversion efficiency in X-ray laser-produced plasmas [40]. For example, at an electron density $n_e = 1.5 \cdot 10^{19}$ cm^{-3} and electron temperatures $T_e = 32$ eV, the abundance of Ar^{+8} is 92% and at $T_e = 110$ eV the abundance of Ar^{+8} is 0.05%. At these conditions, the ionization time of Ar^{+7} to achieve Ne-like Ar^{+8} are $3ns$ ($T_e = 32$ eV) and $0.9ns$ ($T_e = 110$ eV), respectively.

Figure 4 shows the time required for the ionization from Ar^{+6} to Ar^{+7}, Ar^{+7} to Ar^{+8} and Ar^{+8} to Ar^{+9} *versus* electron densities at the optimum electron temperature. It shows that by increasing the electron density by a factor of 10, the ionization time between levels decreases by a factor of 10, as well (the ionization time scales down linearly with electron density).

Figure 5 shows the total ionization time required to achieve each ionic charge level ($Ar^0 \rightarrow Ar^{+Z}$) at constant values of the electron density and temperature of Ne-like Ar^{+8} (Equation (1)). "Total" means the required time to achieve each ionic charge state (Ar^{+Z}). "Total" ionization time, $\sum_{n=1}^{Z} t_{Ar^{+n} \rightarrow Ar^{+(n+1)}}$, comes from the assumption that Ar^0 cannot ionize directly to Ar^{+8}; it should first ionize to Ar^{+1}, then Ar^{+1} ionize to Ar^{+2}, and so forth. In Figure 5, the dashed ellipse shows the range for the pulse duration or the time delay required to achieve Ne-like Ar^{+8}. The t_{ion} to reach Ar^{+8} is 210 ps and to reach Ar^{+9} is 920 ps at the optimal values [30]. This big difference in the ionization

time to reach Ar^{+8} and Ar^{+9} is due to the closed shell configuration at Ne-like. The pre-pulse durations [5–9] and the time delay [10] from the literature are indicated with circles. Figure 5 shows that the pulse durations or the time delay between pulses [5–10] are compatible with the total ionization time for having Ne-like Ar^{+8}.

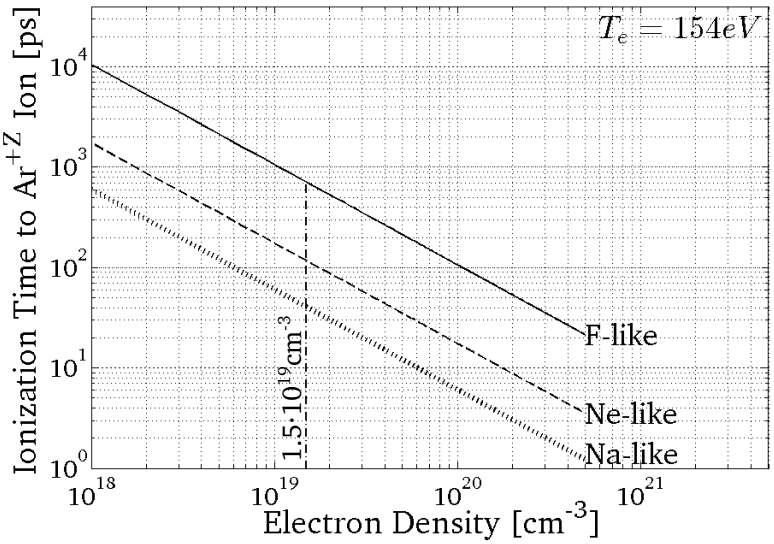

Figure 4. Ionization time to achieve the Ar^{+Z} ion as a function of the electron density at the optimum electron temperature for the following: (i) $Ar^{+6} \rightarrow Ar^{+7}$ (Na-like); (ii) $Ar^{+7} \rightarrow Ar^{+8}$ (Ne-like); and (iii) $Ar^{+8} \rightarrow Ar^{+9}$ (F-like).

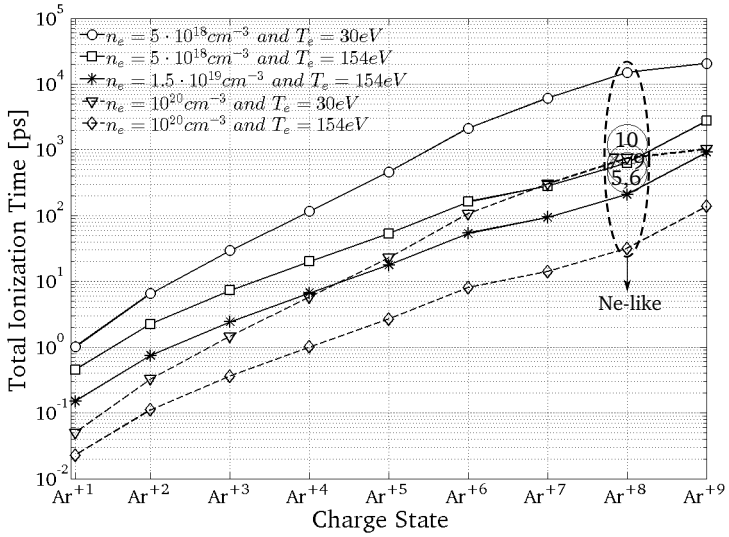

Figure 5. Total ionization time to reach different ionization stages ($Ar^0 \rightarrow Ar^{+Z}$) at different electron densities and temperatures. Namely, the dashed ellipse shows a range for the required total ionization time to achieve Ne-like Ar^{+8} at different electron densities and temperatures. Inside the ellipse, the pre-pulse durations or the time delay between pulses from the literature [5–10] are indicated.

The lasing can be efficient if the pulse duration or the time delay between pre-pulses is comparable with the time required to reach the desired ionic charge level (Ar^{+8}), as shown in Figure 5.

The total ionization time is faster than the cooling characteristic time of the plasma at the optimum electron density and temperature. The cooling characteristic time is ≈823 ps (Equation (2)), which is ≈4-times longer than the total ionization time to achieve Ne-like Ar^{+8} at the optimum electron density and temperature (see Table 2).

By fitting a set of data (see Figure 5), we can predict the required total ionization time for having Ne-like Ar^{+8}, with the electron temperature and electron density dependency as follows:

$$t_{ion}[s] \simeq \frac{(1.4 \pm 0.4) \cdot 10^{13}}{n_e {T_e}^{1.61}} \quad (15)$$

where n_e is in cm^{-3} and T_e is in eV. Equation (15) is obtained for a variety of ranges of electron temperatures and electron densities. In Equation (15), $+0.4$ stands for $T_e < 45$ eV and -0.4 stands for $T_e \gtrsim 45$ eV. The former work [41] had scaled the ionization time of Ne-like Ar^{+8}, which does not have electron temperature dependency.

In the next step, we obtained the transition time between excited levels of Ne-like Ar^{+8} as a ground level.

4.1.3. Transition Times among Ne-Like Levels

Transitions times between Ne-like levels were calculated by considering transient collisional excitations and radiative decays.

Figure 6a shows the transition time between levels composed of an upper (2) and a lower (1) laser level and the ground (0) level at the optimum electron density [30] in the electron temperature range of $T_e = 10$ eV to 2,000 eV. It shows that with increasing the temperature by a factor of five, the transition time from the upper to the lower laser level (τ_{21}) and the transition time from the upper level to the ground state (τ_{20}) are increasing by a factor of 1.8 and 2.4, respectively.

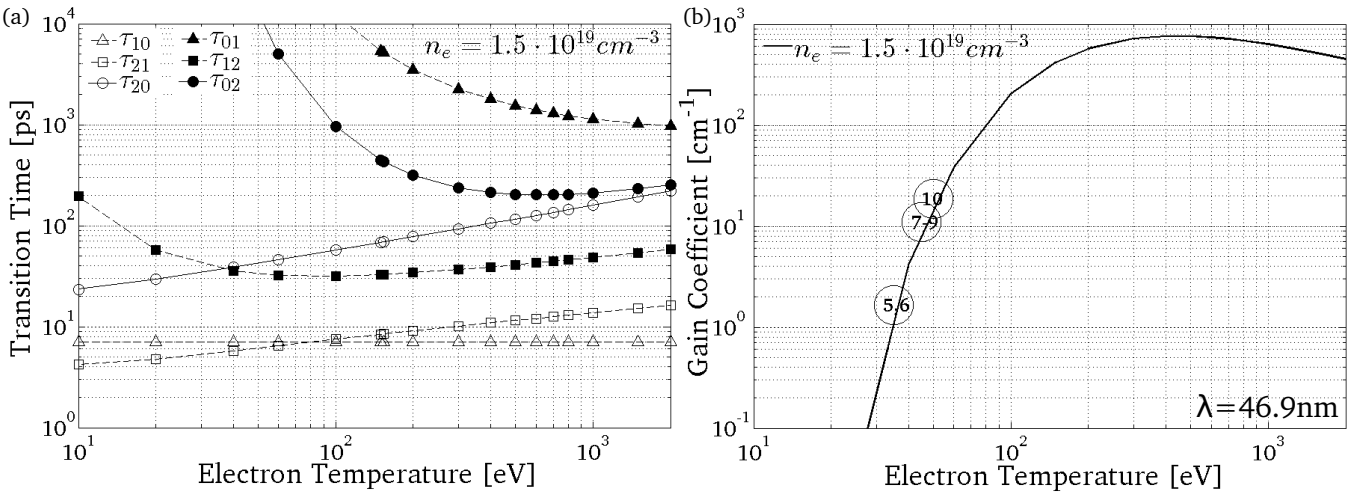

Figure 6. (**a**) Transition time (Equation (3)) between Ne-like Ar^{+8} levels (Figure 1) at the optimum electron density of $1.5 \cdot 10^{19}$ cm^{-3} [30] as a function of temperature. (**b**) Gain coefficient of the Ne-like Ar^{+8} laser at a wavelength $\lambda = 46.9$ nm. Benchmarking data [5–10] from the literature (numbered circles) from experiments for gain coefficients of Ne-like Ar^{+8} laser-produced plasma are given.

It is shown that the transition time from the ground level to the upper level (τ_{02}) and the transition time from the lower to upper level (τ_{12}) are decreasing with increasing the temperatures up to 600 eV and 100 eV, respectively. However, τ_{02} and τ_{12} start to increase for $T_e > 600$ eV and $T_e > 100$ eV, respectively.

Figure 6b shows the calculated gain coefficient of a Ne-like Ar^{+8} at a wavelength $\lambda = 46.9$ nm in the $2p^5 3p^1 (J = 0) \rightarrow 2p^5 3s^1 (J = 1)$ laser transition ($2 \rightarrow 1$) at the optimum electron density [30] *versus* electron temperature. At $T_e = 50$ eV, the gain coefficient is 15 cm^{-1}, while τ_{21} is faster than τ_{10} by a factor of 1.1. Then, a comparison of Figure 6a,b shows that in the transient electron collisional excitation scheme, inversion (gain formation) happens because the collisional excitation and de-excitation processes of the upper and lower levels occur at different rates. The previous claim [42,43] of the faster radiative decay of the lower level than the upper level ($A_{10} > A_{21}$) is thus one aspect of the lasing.

It is shown that at the optimum electron density with increasing the temperatures up to 400 eV, the gain is increasing. If the temperature increases from 35 eV to 400 eV, the gain increases by 2.88-orders of magnitude. At $T_e \approx 35$ eV, the gain coefficient is $\approx$1 cm^{-1}. From $T_e > 400$ eV, the gain starts to decrease.

In Figure 6b, the benchmarking data [5–10] from the experiments for gain coefficients of Ne-like Ar^{+8} produced by the laser-plasma interaction are shown (see Table 1). They are shown just to demonstrate that the experimentally measured gain is always lower than the gain calculated by the theory (atomic calculation). In the experiments, the gain along its propagation path through the plasma suffers from a finite gain lifetime, traveling-wave velocity mismatch or inhomogeneous plasma conditions. All of these effects decrease the measured gain coefficient in the experiment.

Next, we estimate the pumping time *versus* the relaxation time among excited levels of Ne-like Ar^{+8}.

4.1.4. Pumping Time *versus* Relaxation Time among Ne-Like Levels

Since the time it takes to maintain the inversion is equal to the upper level lifetime (the relaxation time of the upper level), the optimum value of the pulse duration of the main pulse must be equivalent to the relaxation time of the upper level (t_{rel2}). However, if the pulse duration of the main pulse is much longer than the lifetime of the upper level, most of the possible inversions would be lost by spontaneous emission without amplification.

Figure 7 shows that the pumping to the upper and lower laser level, as well as the relaxation from the upper and lower level occur at different time scales. In Figure 7a, for plotting the pumping time to the lower and upper level, the optimum value of the upper level population was considered $n_2 = 3 \cdot 10^{-4} n_0 (\lambda_{21})^{0.5}$ [30], where λ_{21} is an X-ray wavelength in angstroms. The population of the upper and lower level is calculated with considering $F = 50\%$ and $F = 10\%$ (Equation (7)). These values of $F = 50\%$ and $F = 10\%$ are conservative values.

It is shown that the relaxation time does not depend on the upper and lower level population, *i.e.*, the relaxation time for both $F = 10\%$ and $F = 50\%$ are the same.

Figure 7a shows that at temperatures higher than 36 eV, corresponding to $F = 10\%$, the pumping time to the upper level is faster than the pumping to the lower level as high as a factor of $\approx$10.

Besides, it is shown that at temperatures higher than 72 eV, corresponding to $F = 50\%$, the pumping time to the upper level is faster than the pumping time to the lower level as high as a factor of $\approx$7.

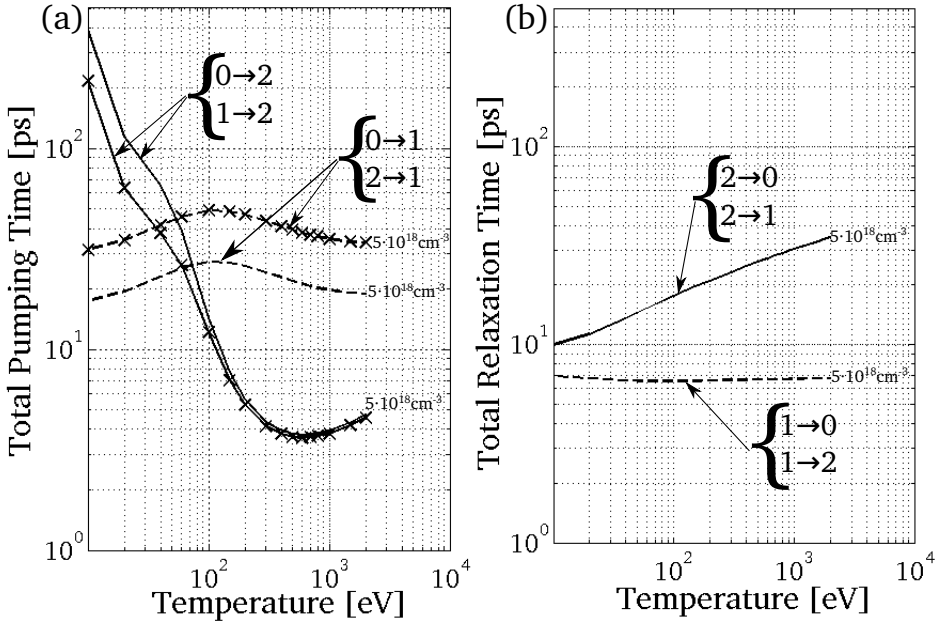

Figure 7. (**a**) Total pumping time (Equation (14a)) to the upper level (2) and lower level (1) at an electron density of $5 \cdot 10^{18}$ cm^{-3}, considering an inversion factor of 10% (curve with marker) and 50% (curve without marker). (**b**) Total relaxation time (Equation (14b)) of the upper (solid line) and lower (dashed line) levels of Ne-like Ar^{+8}.

Figure 7b shows that at an electron density of $5 \cdot 10^{18}$ cm^{-3}, the relaxation time from the lower level is faster than the upper level by a factor of as high as 5.2. It is shown that the relaxation time from the upper level with increasing of the electron temperature at a constant electron density is getting slower. For an electron density of $5 \cdot 10^{18}$ cm^{-3} and electron temperatures in the range of 10 →2000 eV, the relaxation time from the upper level is in the range of $10 \rightarrow 35$ ps.

Figures 5 and 7 show that at a low electron temperature, $T_e = 30$ eV and the electron density $n_e = 5 \cdot 10^{18}$ cm^{-3}, the time scale in which the relaxation time from the upper level ($t_{rel2} \approx 12$ ps) and the lower level ($t_{rel1} \approx 7$ ps) occurs is much lower than the time required to achieve Ne-like ions (t_{ion} ≈15,000 ps) and the time required to generate a population inversion ($t_{pum2} \approx 60$ ps).

Table 2 shows that at an optimum electron density of $1.5 \cdot 10^{19}$ cm^{-3} and increasing the electron temperature by a factor of five, the relaxation time from the upper level is getting slower by a factor of ≈1.7 ($T_e = 154$ eV is an optimum electron temperature [30]). Meanwhile, at a constant electron temperature of $T_e = 30$ eV, increasing the electron density, the relaxation time from the upper level is getting faster. With increasing the electron density by a factor of ≈3, the relaxation time from the upper level is faster by a factor of ≈3.

Table 2. Summary of the effects of the electron temperature and density on t_{ion} (total ionization time to achieve Ne-like ions), t_{pum2} (total pumping time to the upper level) and t_{rel2} (total relaxation time from the upper level) at a wavelength $\lambda = 46.9$ nm in the $2p^5 3p^1 (J = 0) \rightarrow 2p^5 3s^1 (J = 1)$ laser transition at $F > 0$.

n_e (cm^{-3})	T_e(eV)	t_{ion}(ps)	t_{pum2}(ps)	t_{rel2} (ps)	t_{pum2}/t_{rel2}
$1.5 \cdot 10^{19}$	30	5,000	15	4.5	3.3
$1.5 \cdot 10^{19}$	154	211	2.3	7.5	0.3
$5 \cdot 10^{19}$	30	1,500	8	1.4	5.7

Table 2 summarizes the effect of the electron temperature and density on t_{ion}, t_{pum2} and t_{rel2} time scales. It shows that the ratio of t_{pum2} to t_{rel2} is smaller for larger electron temperatures. Implementation data in Table 2 show that, with increasing electron density, both values of t_{rel2} and t_{pum2} are decreasing. Meanwhile, with increasing electron temperature, the value of t_{rel2} and t_{pum2}, respectively, increases and decreases.

Based on our calculation (using Equation (14)), we can estimate the total relaxation time from the upper level (t_{rel2}) and the total pumping time to the upper level (t_{pum2}) for $T_e \lesssim 300$ eV:

$$t_{rel2}[s] \simeq \frac{(2.8 \pm 0.2) \cdot 10^7}{n_e {T_e}^{-0.27}}$$
$$t_{pum2}[s] \simeq \frac{(2.2 \pm 0.3) \cdot 10^{10}}{n_e {T_e}^{1.23}} \quad (16)$$

where n_e is in cm^{-3} and T_e is in eV. Equation (16) is retrieved by fitting the data points by considering a specific electron density and temperature and taking into account Ne-like Ar^{+8} as a ground level (see Figure 1).

So far, the electron density and temperature influence the total ionization time required to obtain Ne-like Ar^{+8} and also affect the time scales of t_{pum} and t_{rel}. In the next section, we show how the pulse duration can influence the quantity of the electron density and temperature in the X-ray-produced plasma.

4.2. Effect of Pulse Duration on Hydrodynamic Parameters

In order to determine the dependency of the pulse duration on the electron density and temperature of the laser-produced plasma, we studied the evolution of the electron density and temperature produced by different pulse durations.

Figure 8 shows the maximum electron temperature and maximum electron density *versus* time in the direction of plasma expansion. The data in Figure 8 are obtained from our calculation using a hydro-code (Hyades).

During the short laser pulse, little expansion occurs ($L_{exp} = v_{exp} \cdot \Delta\tau_p$). This allows the direct deposition of a remarkable amount of the laser energy on the plasma, which means a higher electron temperature.

It is found that the electron density and temperature are respectively a factor of ≈2.1- and ≈5-times higher in the case of a shorter pulse of $\Delta\tau_p = 0.1$ ps in comparison to the long pulse of $\Delta\tau_p = 1{,}000$ ps.

Implementation Figure 8 and data in Table 2 show that in the case of a shorter pulse, the time required for producing Ne-like Ar^{+8} and the t_{pum2} and t_{rel2} time scales will be shorter and closer together.

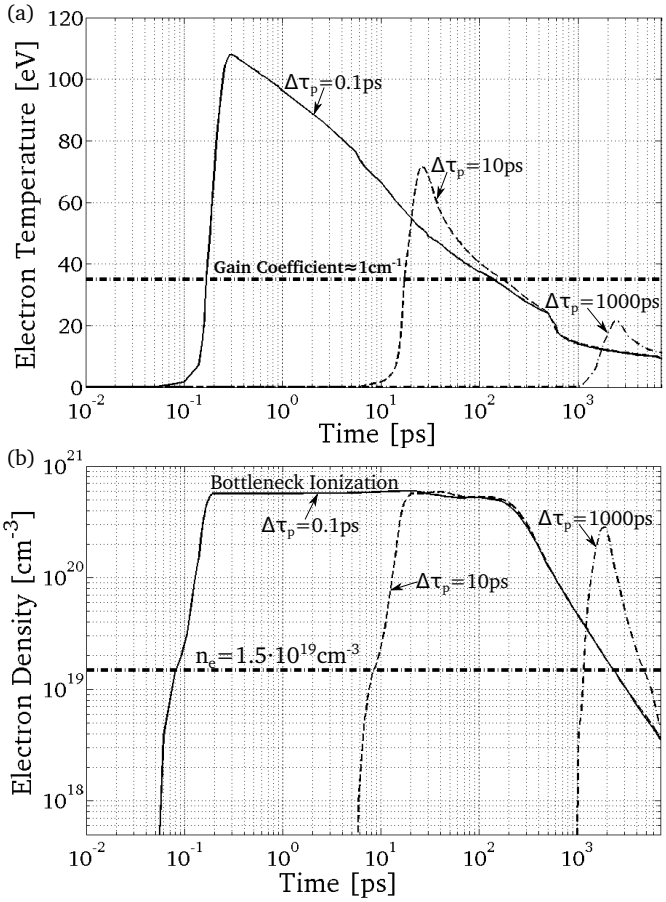

Figure 8. (**a**) Time-dependent electron temperature and (**b**) electron density produced with pulses with durations of 0.1 ps, 10 ps and 1,000 ps and energy fluence $j_L \approx 10$ J/cm^2.

Figure 8b shows that in the case of the plasma produced with the pulse duration of 0.1 ps, there is a bottleneck in the ionization level at $0.2ps \lesssim t \lesssim 4$ ps, which means that plasma for recombination and expansion needs more time. Figure 8a shows that electrons can lose energy emitting radiation and by conduction, so the temperature diminishes. Ne-like Ar^{+8} is the closed shell, making removal of an additional electron more difficult. This significantly increases the threshold for further electron ionization, which can also be considered an ionization bottleneck for a plasma at a specific temperature.

Figure 8b shows that the electron density is always less than $n_{ec} \approx 10^{21}$ cm^{-3}, where n_{ec} is the critical electron density and also a turning point in the normal incidence for the pump laser with a wavelength $\lambda = 1{,}054$ nm. Figure 8b shows that the plasma produced by a gas target can limit the refraction of the pump-pulse, which means the time delay between pulses cannot be an issue in order to smear-out the electron density gradient.

The line cross of optimum electron density is shown in Figure 8a, and the gain coefficient of ≈ 1 cm^{-1} at this optimum electron density and electron temperature 35 eV is shown in Figure 8b. Figure 8b shows that the plasma produced by the long pulse $\Delta\tau_p = 1{,}000$ ps is below the area with the gain coefficient of 1 cm^{-1}.

4.3. Optimum Pump-Laser Intensity for Achieving Ne-Like Ar^{+8}

In this section, the optimum pump-laser intensity at the focus point of the laser on the target in order to have Ne-like Ar^{+8} is estimated.

Figure 9 shows the optimum laser intensity required to have Ne-like Ar^{+8} at different pulse durations and Ar^0 mass densities, obtained from the hydro-code (Hyades). It shows that with increasing the initial gas density by a factor of 10, the required laser intensity is decreased by a factor as high as ≈7. When charged particles are accelerated in the electric field of the laser, they can ionize neutral gas molecules by collisions. Then, the process is dependent on the initial gas density (pressure).

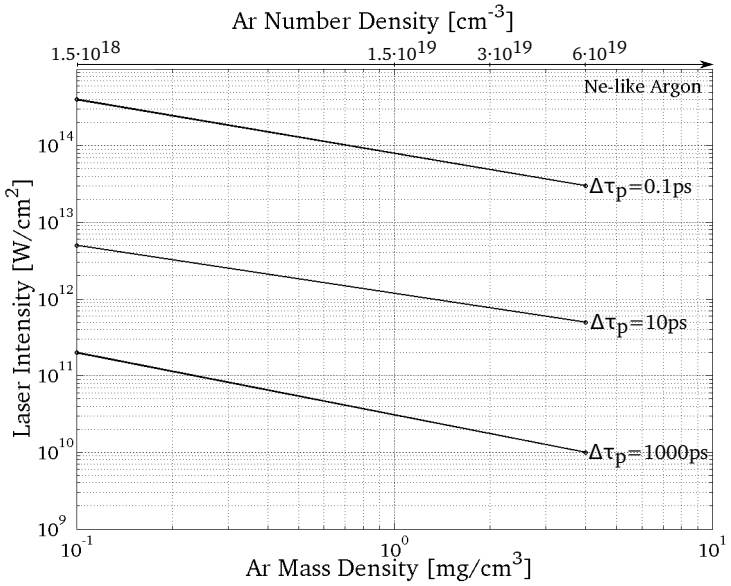

Figure 9. Optimum laser intensity for having Ne-like Ar^{+8} as a function of Ar^0 density at different pulse durations. The top axis is the number density (cm^{-3}).

Based on the results in Figure 9 and by the method of curve fitting from MATLAB code, the following power-law formula can be obtained:

$$
\begin{aligned}
I_{opt}(W/cm^2) &\approx \Delta\tau_p^{-1.13}\left(\frac{5.81\cdot 10^{12}}{\rho_0^{0.72}}\right),\ \Delta\tau_p < 1ps \\
I_{opt}(W/cm^2) &\approx \Delta\tau_p^{-1.01}\left(\frac{1.24\cdot 10^{13}}{\rho_0^{0.59}}\right),\ 1 \leqslant \Delta\tau_p \leqslant 100ps \\
I_{opt}(W/cm^2) &\approx \Delta\tau_p^{-0.31}\left(\frac{2.78\cdot 10^{11}}{\rho_0^{0.79}}\right),\ \Delta\tau_p > 100ps
\end{aligned}
\tag{17}
$$

where the optimum pump-laser intensity (I_{opt}) for having Ne-like Ar^{+8} has dependency on the pulse duration and initial Ar^0 density. In Equation (17), $\Delta\tau_p$ is the pulse duration in ps and ρ_0 is the initial Ar^0 mass density in mg/cm^3.

5. Conclusions

In this study, we systematically investigated the optimum time configuration of pump pulses.

In Section 4.1.2, we studied a neutral Ar^0 ionization time scale for achieving Ne-like Ar^{+8}. We found that the dielectronic recombination has an important effect at temperatures less than 50 eV. For $T_e \lesssim 50$ eV, without considering dielectronic recombination, the ionization time is overestimated as high as a factor of 30. For $T_e > 50$, this difference reduces to 14%.

The total ionization time in order to achieve Ne-like ions is obtained by Equation (15).

In Section 4.1.3, we showed that in the transient electron collisional pumping scheme, lasing happens because the collisional excitation processes of the upper and lower levels occur at different rates, and not simply because of the faster rate of the radiative decay of the lower level. Thus, even if the transition time of the upper level (2) to the lower level (1) is faster than the transition time from the lower level (1) to the ground state (0), the gain coefficient can appear.

In Section 4.1.4, we demonstrated that at low temperatures ($T_e = 30$ eV) and at certain an electron density ($n_e = 1.5 \cdot 10^{19}$ cm^{-3}), both the total relaxation time from the upper level (4.5 ps) and total pumping time to the upper level (15 ps) are much shorter than the time required to achieve Ne-like ions (5000 ps).

In Section 4.1.4, we showed that the ratio of the pumping time for the population inversion to the relaxation time from the upper level can be as high as a factor of 10 for $T_e \gtrsim 20$ eV, depending on the electron density.

We found that at temperatures higher than 36 eV ($F = 10\%$) and 72 eV ($F = 50\%$), the upper level will be pumped faster than the lower level by a factor as high as 10.

It is shown that at a constant electron density ($1.5 \cdot 10^{19}$ cm^{-3}), increasing the temperature by a factor of five ($30 \rightarrow 154$ eV), the ionization time to achieve Ne-like ions and the pumping time to the upper level are decreasing, by a factor of 24 and 6.5, respectively. Meanwhile the relaxation time from the upper level is increasing by a factor of 1.7 (Table 2).

It is found that at a constant electron temperature (30 eV), increasing the electron density by a factor of 3.3 ($1.5 \cdot 10^{19} \rightarrow 5 \cdot 10^{19}$ cm^{-3}), all time scales including ionization time, pumping time and relaxation time to the upper level are decreasing, by a factor of 3.3, 1.9 and 3.2, respectively (Equation (16)).

Besides, the pumping time to the upper level (2) and relaxation time from the lower level (1) are estimated; Equation (16). It was found that for an electron density higher than $5 \cdot 10^{18}$ cm^{-3}, at electron temperatures in the range $10 \rightarrow 2000$ eV, the relaxation time from the upper level is as high as $\tau_{rel2} \leq 35$ ps. The most effective lasing happens with short pulses with a pulse duration comparable to the total relaxation time from the upper level, namely $\Delta\tau_p \leq 35$ ps.

In Section 4.2, we studied the effect of the pulse duration on the electron temperature or density for plasma lasing. The optimum time scale required to achieve Ne-like ions, as well as the time required to generate a population inversion depends on the combined effect of the temperature and density (Table 2).

In Section 4.3, a formula for calculating optimum laser intensity for producing the Ne-like Ar^{+8} is obtained; Equation (17). This equation can be used for different pulse durations and considering different initial gas densities of Ar^0.

Acknowledgments

The authors acknowledge discussions with Dr. Eduardo Oliva (Universite Paris-Sud).

The present work was supported by the Swiss National Science Foundation under Grant Number PP00P2-133564/1.

Author Contributions

The work is a part of L.M.'s PhD studies under supervision of D.B.

Conflicts of Interest

The authors declare no conflict of interest.

References

1. Dunn, J.; Keenan, R.; Shlyaptsev, V.N. Soft X-Ray Lasers and Applications VI. *Proc. SPIE* **2005**, *5919*, 35–42.
2. Masoudnia, L.; Bleiner, D. *Laser Phys.* **2013**, *23*, 056003.
3. Oliva, E.; Zeitoun, P.; Sebban, S.; Fajardo, M.; Velarde, P.; Cassou, K.; Ros, D. *Opt. Lett.* **2009**, *34*, 2640–2642.
4. Davidkova, M.; Juha, L.; Bittner, M.; Koptyaev, S.; Hajkova, V.; Krasa, J.; Pfeifer, M.; Stisova, V.; Bartnik, A.; Fiedorowicz, H.; *et al*. *Radiat. Res.* **2007**, *168*, 382–387.
5. Fiedorowicz, H.; Bartnik, A.; Li, Y.; Lu, P.; Fill, E. *Phys. Rev. Lett.* **1996**, *76*, 415–418.
6. Fiedorowicz, H.; Bartnik, A.; Kostecki, J.; Szczurek, M.; Fill, E.; Li, Y.; Lu, P.; Pretzler, G.; Nilsen, J. X-Ray Lasers 1996. In Proceedings of the Fifth International Conference on X-Ray Lasers, Lund, Sweden, 10-14 June 1996.
7. Dunn, J.; Smith, R.F.; Nilsen, J.; Fiedorowicz, H.; Bartnik, A.; Shlyaptsev, V.N. *J. Opt. Soc. Am. B* **2003**, *20*, 203–207.
8. Fiedorowicz, H.; Bartnik, A.; Dunn, J.; Smith, R.F.; Hunter, J.; Nilsen, J.; Osterheld, A.L.; Shlyaptsev, V.N. *Opt. Lett.* **2001**, *26*, 1403–1405.
9. Fiedorowicz, H.; Bartnik, A. *Bull. Pol. Acad. Sci.: Tech. Sci.* **2005**, *53*, 103–111.
10. Lu, P.; Kawachi, T.; Suzuki, M.; Sukegawa, K.; Namba, S.; Tanaka, M.; Hasegawa, N.; Tai, R.; Kishimoto, M.; Kado, M.; *et al*. Photon energy conversion from IR femtosecond laser pulses to X-ray pulses with electrolyte aqueous solutions in air. *AIP Conference Proc.* **2002**, *634*, 260.
11. Rocca, J.J.; Shlyaptsev, V.; Tomasel, F.G.; Cortazar, O.D.; Hartshorn, D.; Chilla, J.L.A. *Phys. Rev. Lett.* **1994**, *73*, 2192–2195.
12. Oepts, D.; van der Meer, A.F.G.; van Amersfoort, P.W. *Infrared Phys. Technol.* **1995**, *36*, 297–308.
13. Filipponi, A.; Borowski, M.; Bowron, D.T.; Ansell, S.; di Cicco, A.; de Panfilis, S.; Itie, J.P. *Rev. Sci. Instrum.* **2000**, *71*, 2422–2432.
14. Linford, G.J.; Peresini, E.R.; Sooy, W.R.; Spaeth, M.L. *Appl. Opt.* **1974**, *13*, 379–390.
15. Masoudnia, L.; Bleiner, D. *Nucl. Inst. Methods Phys. Res. B* **2014**, *323*, 59–70.
16. Gu, M.F. The Flexible Atomic Code (FAC). *Can. J. Phys.* **2008**, *86*, 675–689.
17. Bitter, M.; Gu, M.F.; Vainshtein, L.A.; Beiersdorfer, P.; Bertschinger, G.; Marchuk, O.; Bell, R.; LeBlanc, B.; Hill, K.W.; Johnson, D.; *et al*. *Phys. Rev. Lett.* **2003**, *91*, 265001.
18. Wang, X.L.; Dong, C.Z.; Su, M.G. *Nucl. Inst. Methods Phys. Res. B* **2012**, *280*, 93–97.

19. May, M.J.; Beiersdorfer, P.; Jordan, N.; Scofield, J.H.; Reed, K.J.; Hansen, S.B.; Fournier, K.B.; Gu, M.F.; Brown, G.V.; Porter, F.S.; *et al*. *Nucl. Inst. Methods Phys. Res. B* **2005**, *235*, 231–234.
20. Aggarwal, K.M.; Keenan, F.P. *At. Data Nucl. Data Tables* **2013**, *99*, 156–248.
21. Chung, H.K.; Chen, M.H.; Morgan, W.L.; Ralchenko, Y.; Lee, R.W. FLYCHK Site. Available online: http://nlte.nist.gov/FLY/ (accessed on 28 January 2015).
22. Chung, H.K.; Chen, M.H.; Morgan, W.L.; Ralchenko, Y.; Lee, R.W. *High Energy Density Phys.* **2005**, *1*, 3–12.
23. Larsen, J.T. *Hyades- A Plasma Hydrodynamics Code for Dense Plasma Studies*; Cascade Applied Sciences, Inc.: Longmont, CO, USA, 1990.
24. McWhirter, R. *Plasma Diagnostic Techniques*; Huddlestone, R., Leonard, S., Eds.; Academic Press: New York, NY, USA, 1965; Chapter 5, pp. 201–264, .
25. Pert, G.J. *Phys. Rev. A.* **2006**, *73*, 033809.
26. Hicks, A.K.; Canizares, C.R. *Astrophys. J.* **2001**, *556*, 468–470.
27. Salzmann, D. *Atomic Physics in Hot Plasmas*; Oxford University Press: New York, NY, USA, 1998.
28. Kolb, A.C.; McWhirter, R.W.P. *Phys. Fluids* **1964**, *7*, 519–531.
29. Eidmann, K. *Laser Part. Beams* **1994**, *12*, 223–244.
30. Elton, R.C. *X-Ray Lasers*; Academic Press, Inc.: London, UK, 1990.
31. Regemorter, H.V. *J. Astrophys.* **1962**, *136*, 906.
32. Huba, J.D. *NRL Plasma Formulary*; Naval Research Laboratory: Washington, DC, USA, 1994.
33. Oliva, E.; Zeitoun, P.; Velarde, P.; Fajardo, M.; Cassou, K.; Ros, D.; Sebban, S.; Portillo, D.; le Pape, S. *Phys. Rev. E* **2010**, *82*, 056408.
34. Cassou, K.; Zeitoun, P.; Velarde, P.; Roy, F.; Ogando, F.; Fajardo, M.; Faivre, G.; Ros, D. *Phys. Rev. A* **2006**, *74*, 045802.
35. Attwood, D. *Soft X-rays*; Cambridge Uni Press: New York, NY, USA, 1999.
36. Griem, H.R. *Principle of Plasma Spectroscopy*; Cambridge University Press: New York, NY, USA, 1997.
37. Zeng, X.; Mao, X.; Mao, S.S.; Yoo, J.H.; Greif, R.; Russo, R.E. *Appl. Phys.* **2004**, *95*, 816–822.
38. Olivero, J.J.; Longbothum, R.L. *J. Quant. Spectrosc. Radiat. Transf.* **1977**, *17*, 233–236.
39. Voronov, G.S. *At. Data Nucl. Data Tables* **1997**, *65*, 1–35.
40. Kauffman, R.L.; Phillion, D.W.; Spitzer, R.C. *Appl. Opt.* **1993**, *32*, 6897–6900.
41. Masnavi, M.; Nakajima, M.; Horioka, K. *Appl. Phys.* **2004**, *95*, 434–437.
42. Hagelstein, P.L. Short Wavelength Lasers: Something New, Something Old. OSA Proceeding on Short Wavelength Coherent Radiation: Generation and Applications; Falcone, R. W.; Kirz, J., Ed.; Volume 2, pp. 28–35; (Optical Society of America, Washington, DC, USA, 1988).
43. Prasad, Y.B.S.R.; Nigam, S.; Aneesh, K.; Barnwal, S.; Tripathi, P.K.; Naik, P.A.; Navathe, C.P.; Gupta, P.D. *Sadhana Indian Acad. Sci.* **2011**, *36*, 349–355.